nm-Scale Precision Polymer Patterning of PDMS: Multiscale Insights into Patterning Efficiency using Alkyldiynamines

Anni Shi,† Anamika Singh,† Laura Williams,† Juan C. Arango,† and Shelley A. Claridge†,‡,*

†Department of Chemistry, Purdue University, West Lafayette, Indiana 47907
‡Weldon School of Biomedical Engineering, Purdue University, West Lafayette, Indiana 47907
Address correspondence to: claridge@purdue.edu, (phone) 765-494-6070

ABSTRACT: Most high-resolution interfacial patterning approaches are restricted to crystalline inorganic interfaces. Recently, we have shown that it is possible to generate 1-nm-resolution functional patterns on soft materials, such as polydimethylsiloxane (PDMS), by creating highly structured striped patterns of functional alkyldiacetylenes on a hard crystalline surface, photopolymerizing to set the molecular pattern as a striped-phase polydiacetylene (sPDA), and then covalently transferring the sPDAs to PDMS. Transfer depends on the diacetylene polymerization, making it important to understand design principles for efficient sPDA polymerization and crosslinking to PDMS. Here, we combine single-molecule and fluorescence-based metrics for sPDA polymerization and transfer, first to characterize sPDA polymerization of amine striped phases, then to develop a probabilistic model that describes the transfer process in terms of sPDA–PDMS crosslinking reaction efficiency and number of reactions required for transfer. We illustrate that transferred patterns of alkylamines can be used to direct both adsorption of CdSe nanocrystals with alkyl ligand shells, and covalent reactions with fluorescent dyes, highlighting the utility of functional patterning of the PDMS surface.

Keywords: polydimethylsiloxane, monolayers, two-dimensional materials, polydiacetylene, surface chemistry, chemical patterning

INTRODUCTION

Materials with designed chemical environments near the atomic scale are important in areas ranging from electronics and quantum computing[1-2] to regenerative medicine.[3] Approaches to designed molecular-scale chemical features at material interfaces have often relied on the lattice structure of a pristine inorganic surface to control placement of functional groups.[4-8] However, many emerging applications, including those in wearable electronics[9-10] and regenerative medicine,[11] require chemical patterning of soft, amorphous surfaces. Such materials often express significant structural heterogeneties over length scales of tens to hundreds of nanometers or more, making it challenging to control molecular-scale placement on the surface.

Recently, we have demonstrated that it is possible to design nanometer-resolution chemical patterns on crystalline surfaces,[8,12-13] and transfer the sub-nanometer-thick surface layer to polydimethylsiloxane (PDMS), an amorphous substrate.[14-16] This approach allows us to pattern chemical structure an order of magnitude below the length scale of heterogeneity of the amorphous material. Our method takes advantage of an unusual striped-phase monolayer structure of amphiphiles that assembles noncovalently on highly oriented pyrolytic graphite (HOPG), graphene, and other 2D materials (*e.g.* MoS_2). In the striped phase, alkyl chains orient parallel to the substrate (Figure 1a), forming 1-nm-wide rows of functional groups separated by ~5-nm-wide stripes of exposed alkyl chains.[17] Striped phases in which the monomers include an internal diacetylene can undergo UV photopolymerization, forming conjugated polydiacetylene (PDA) backbones.[18-20] Classically, such phases have been studied with an interest in molecular electronics,[21-22] due to the delocalization of electrons in the striped-phase PDA (sPDA). However, the sPDA backbone can also tether together patterned functional groups for covalent transfer of the molecular pattern to materials such as PDMS.[14]

The monolayer transfer process relies on efficient polymerization of the DA monolayer on the 2D substrate. Although there is a signficant body of knowledge regarding DA polymerization in bulk,[23-26] there is limited understanding of the monomer structural features that maximize polymerization efficiency in striped phases. Such understanding is critical for applications, including transfer to PDMS, that rely on high conversion to the sPDA. Recently, we have shown that there is a large difference in polymerization efficiency between the two diynoic acids most commonly used in striped phase assembly.[16] Differences in monomer alkyl chain structure appear to impact the rate of polymer propagation, leading to differences in polymer length.

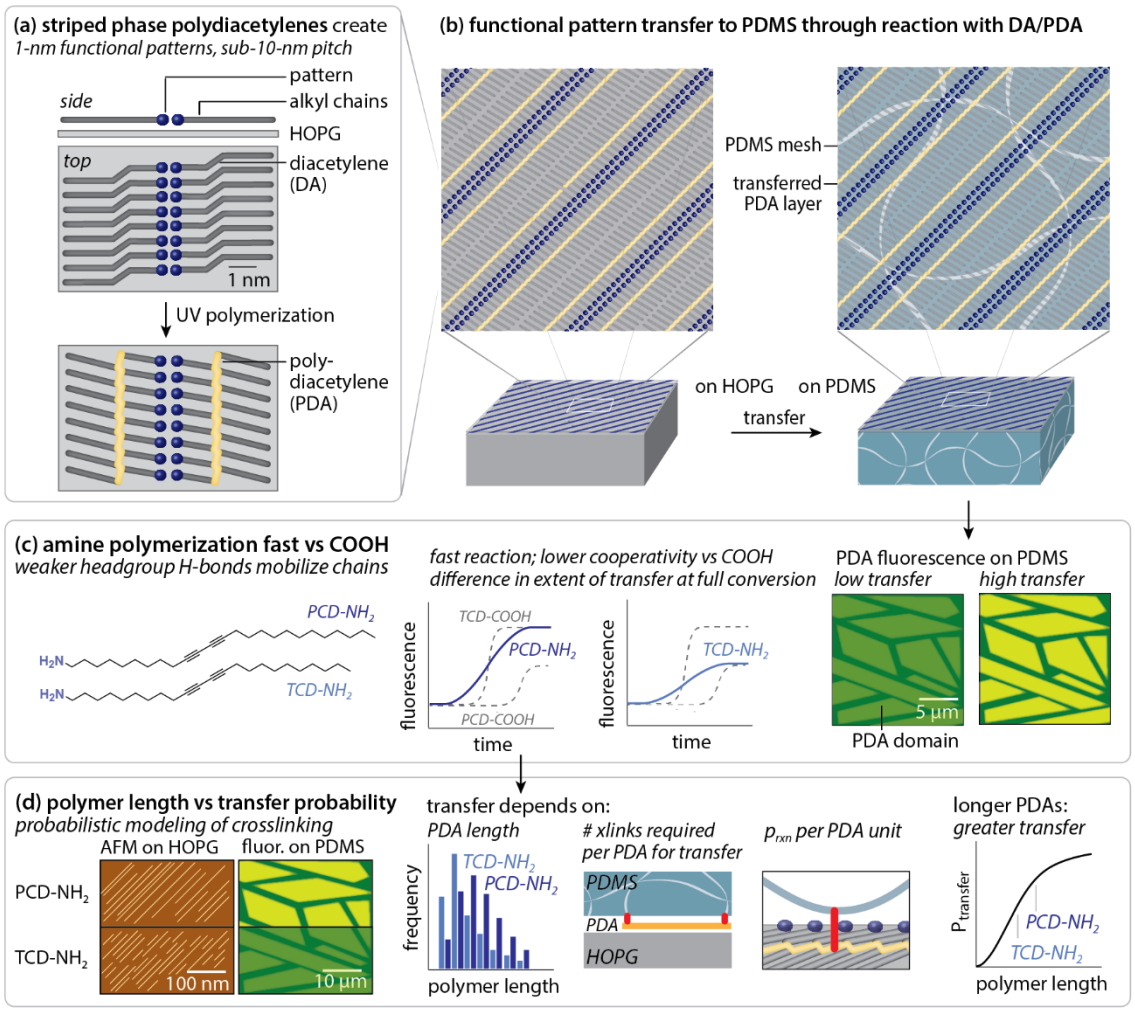

Figure 1. (a) Illustration of striped phase assembly on HOPG and (b) transfer of sPDAs to PDMS for nm-resolution functional patterning. (c) Illustration of use of fluorescence to characterize polymerization kinetics and transfer efficiency of NH_2 sPDAs in comparison with COOH sPDAs. (d) Illustration of probabilistic model for sPDA transfer efficiency.

Here, we extend the understanding of sPDA polymerization and reactive transfer processes in two key ways. First, we examine the role of monomer headgroup H-bonding in polymerization, making comparisons between COOH headgroups (which form strong H-bond dimers between rows) and amines (which have weaker H-bonding). Amine functionalities are especially useful in functional interface design, since primary amines undergo a wide range of reactions,[27-30] allowing for elaboration of the interface chemistry. Overall, the weaker H-bonding between amine headgroups appears to support rapid polymerization. Second, we combine molecular-scale information regarding polymer lengths with microscopic information on extent of transfer, developing a model that relates the probability of sPDA transfer to polymer length. This provides physical insight into the efficiency of the interfacial reaction process that drives sPDA transfer, overcoming challenges associated with spectroscopic characterization of rare reaction events.

RESULTS AND DISCUSSION

Preparation of striped-phase monolayers. To compare polymerization efficiency of alkyl diynamines based on chain structure, we first prepared striped monolayers of 10,12-pentacosadiynamine (PCD-NH_2) and 10,12-tricosadiynamine (TCD-NH_2). Monolayers were assembled through Langmuir-Shaefer (LS) conversion,[31-32] which reorders standing-phase molecules on an aqueous subphase into lying-down striped phases on highly ordered pyrolytic graphite (HOPG). Molecular models of unpolymerized (Figure 2a) and polymerized (Figure 2b) PCD-NH_2 after energy minimization illustrate an edge-to-edge lamellar width of 6.5 nm; in these models, rehybridization of the DA to form the PDA produces a small conformational change that narrows each line, creating a gap between rows of amines, while maintaining the original lamellar edge-to-edge distance (see further discussion later in the manuscript). The modeled lamellar width is in reasonable agreement with the measured periodicity of the striped phase (~6.8 nm) in AFM images (Figure 2c, inset), which also includes the van der Waals distance between chain ends. PCD-NH_2 molecules (Figure 2c,

main image) order epitaxially with the hexagonal HOPG lattice, exhibiting ~120° angles between domains (lamellar axes in two domains labeled with white arrows). TCD-NH_2 assembles into similar domain structures; see Supporting Information Figure S1 for larger AFM images of PCD-NH_2 and TCD-NH_2 monolayers.

Following UV irradiation, polymerized monolayers of PCD-NH_2 exhibit linear features (Figure 2d) with a 0.15-nm topographic protrusion (Figure 2d, inset). These features are consistent with the lifted form of the sPDA observed previously for polymerized lamellar phases of 10,12-pentacosadiynoic acid.[33] Similar structural features are also observed for TCD-NH_2 (Figure S1).

SEM images (Figure 2e) enable characterization of monolayers on HOPG at scales similar to those in fluorescence microscopy images presented in later figures. Regions of bare HOPG

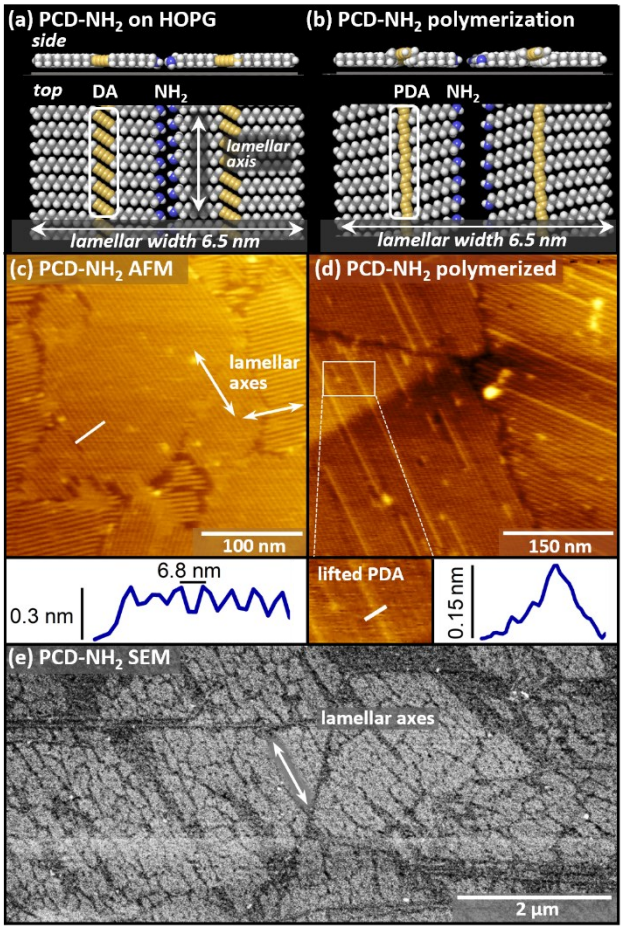

Figure 2. (a, b) Molecular models of (a) unpolymerized and (b) polymerized PCD-NH_2 striped phases on HOPG, highlighting lamellar width. (c, d) AFM images of (c) unpolymerized and (d) polymerized PCD-NH_2. Arrows in (c) illustrate lamellar axes in two domains oriented epitaxially with the HOPG lattice. Inset in (c) is a line scan acquired at the white line segment in (c). Inset in (d) illustrates topographic protrusion corresponding to 'lifted' sPDA backbone. (e) SEM image of PCD-NH_2 domains, showing lamellar axis revealed by cracks in monolayer.

appear darker, due to more limited secondary electron scattering; small defects in molecular domains produced during polymerization elucidate molecular row orientation in large domains (highlighed in image). See Supporting Information Figures S2 and S3 for larger SEM images of TCD-NH_2 and PCD-NH_2 monolayers on HOPG.

Comparison of polymerization of TCD-NH_2 and PCD-NH_2. To understand the impact of the amine headgroups on polymerization, we compared AFM and fluorescence images of polymerized TCD-NH_2 and PCD-NH_2 (Figure 3, Figure S4). AFM images provide molecular-level insight into polymerization, including the lengths of individual polymers. Imaging fluorescence emission from the sPDA backbones provides a complementary ensemble view of the process. Although sPDA fluorescence is quenched on HOPG, we have recently found that polymerized lamellar phases can be transferred to non-quenching PDMS,[14-15] and that emission intensity on PDMS increases with the polymerization conversion on HOPG, for diynoic acids.[16]

Monolayer transfer is carried out by curing PDMS in contact with an sPDA layer on HOPG. PDMS curing involves formation of covalent bonds between vinyl groups in the PDMS base polymer and Si-H groups in the crosslinker, in the presence of a transition metal catalyst (Figure 3a). When carried out in contact with the sPDA layer, C-C multiple bonds in the sPDA can also participate in the reaction, covalently linking the sPDA to the PDMS network. When the PDMS is exfoliated from the HOPG, elements of the monolayer that are covalently linked to the PDMS are transferred from the HOPG. Fluorescence emission from sPDA backbones on PDMS (Figure 3b), can be used to quantify the amount of sPDA transferred, providing a convenient means of estimating photopolymerization kinetics of the sPDA monolayer on HOPG.[16]

Here, we examined polymerization kinetics for amine striped phases on HOPG, preparing sets of TCD-NH_2/HOPG and PCD-NH_2/HOPG substrates, and controlling UV irradiation time in the range from 0–90 min. Following transfer to PDMS, both types of amine sPDAs exhibit sigmoidal trends in fluorescence emission with increasing polymerization time on HOPG (Figure 3c). Local variations in emission intensity are observed (Figure S5-10), consistent with microscale variations in domain structure observed in the monolayers on HOPG; these are reflected in the magnitude of the error bars for the measurements. The sigmoidal trend in emission intensity is consistent with a cooperative polymerization process, in which differences between monomer and polymer unit cells generate strain in the mixed lattice, accelerating polymerization later in the process. Cooperativity is common in bulk polymerization of PDAs,[23,34] and is consistent with our previous observations of TCD-COOH and PCD-COOH sPDA reactions on HOPG.[16] For sPDAs with COOH headgroups, monomers with 10-carbon terminal chain segments exhibited more rapid polymerization,[16] in comparison with diynoic acids with shorter or longer terminal segments, meaning that TCD-COOH polymerizes more rapidly than PCD-COOH (shorter $t_{1/2}$).

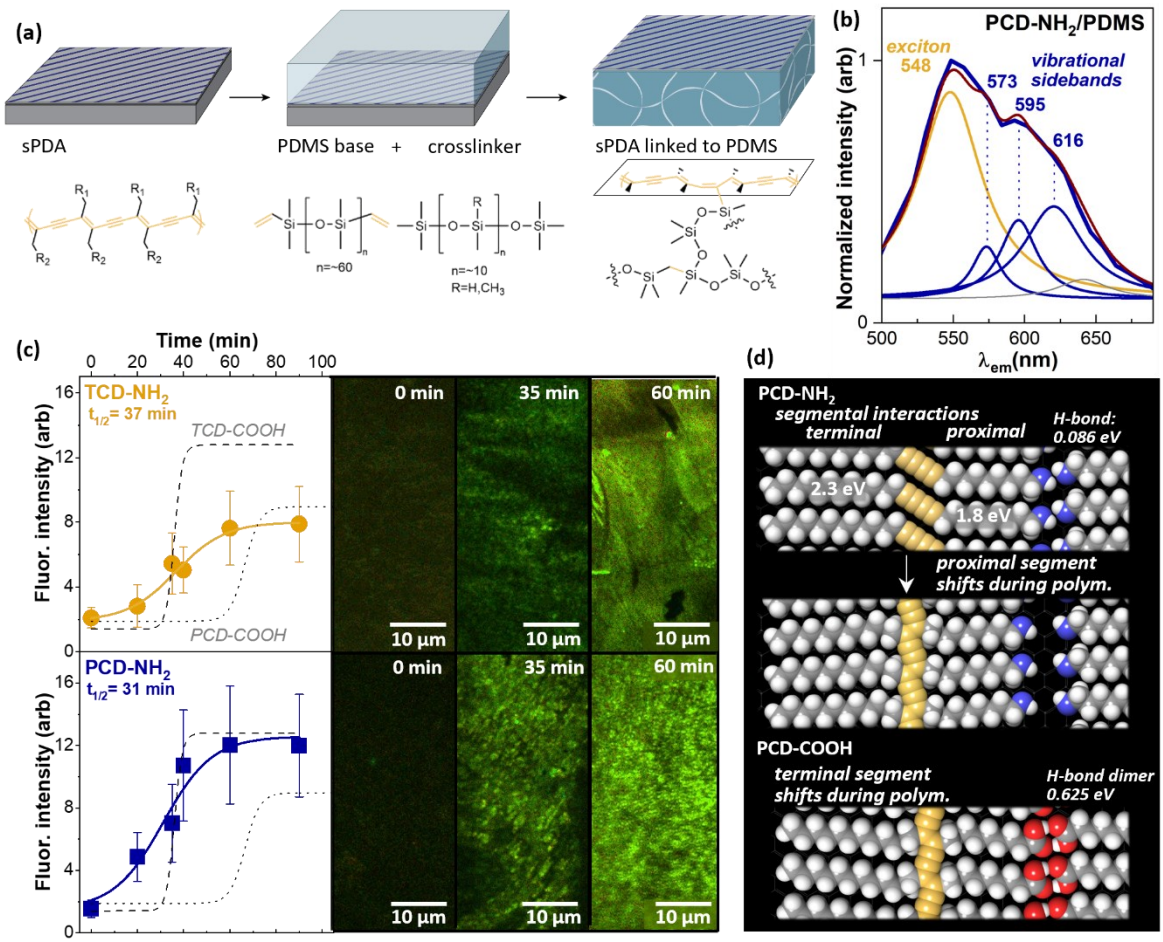

Figure 3. (a) Schematic of sPDA transfer to PDMS. (b) Fluorescence emission spectrum of PCD-NH_2/PDMS showing excitonic peak and vibrational sidebands. (c) Measurement of fluorescence emission for TCD-NH_2 and PCD-NH_2 transferred to PDMS following photopolymerization on HOPG for stated time; curve fits of previously measured values for structurally comparable carboxylic acids (TCD-COOH and PCD-COOH)[16] are shown in dashed and dotted grey lines, respectively. Representative fluorescence images at selected timepoints (0, 35, 60 min) are also shown. (d) Molecular models of conformational change associated with polymerization of PCD-NH_2 (top) and PCD-COOH (bottom). Grey lines in (c) adapted with permission from Reference 16.

However, amine sPDA phases exhibit different behavior. The midpoints of the sigmoidal curves collected here for amines are similar for the two molecules ($t_{1/2}$(PCD-NH_2) = 31 min, $t_{1/2}$(TCD-NH_2) = 37 min); both are similar to our previously observed $t_{1/2}$(TCD-COOH) = 36 min.[16] Additionally, at all points along the curve, PCD-NH_2/PDMS exhibits greater fluorescence emission, consistent with a greater amount of transferred PDA. Maximum fluorescence emission observed here for PCD-NH_2 is similar to that observed previously for TCD-COOH, while the maximum for TCD-NH_2 is similar to that for PCD-COOH.

For COOH-sPDAs, strong hydrogen-bonded COOH dimers constrain the movement of the chain segment proximal to the headgroups during polymerization (Figure 3d, bottom). Therefore, the terminal segment structure determines PDA conformation and polymerization efficiency. For diynamines, the weaker H-bonding between amine headgroups decreases interaction strength between proximal chain segments. Segmental interactions of proximal and terminal chain segments are calculated using the following values: $CH_2\cdots\pi$ (125 meV), $CH_2\cdots CH_2$(63 meV) and $NH_2\cdots NH_2$ (86 meV),[35] resulting in segmental values of E_{prox} = 1.8 eV (for both PCD-NH_2 and TCD-NH_2), E_{term}(PCD-NH_2) = 2.3 eV and E_{term}(TCD-NH_2) = 1.9 eV. This suggests that, during polymerization, motion of the proximal chain segment (Figure 3d, center) is slightly favored. At higher humidity levels, differences in headroup hydration may also contribute to differences in segmental interactions, impacting polymerization, and it it possible that over longer timescales, molecular motion allows H-bonds to reform.

The slope of the vertical section of the sigmoidal curve is often used as a metric for cooperativity in topochemical polymerization of PDAs in bulk.[36] Here, for both PCD-NH_2 and TCD-NH_2, polymerization is rapid (in comparison to COOH sPDAs), exhibiting a short $t_{1/2}$. However, the slopes of the sigmoidal curves for TCD-NH_2 and PCD-NH_2 are 0.14 and 0.26, respectively, notably lower than those for the equivalent diynoic acids (0.72 for TCD-COOH and 0.58 for PCD-COOH); this is consistent with decreased cooperativity due to weaker H-bonding interactions between headgroups.

Impact of terminal segments on chain propagation. Next, we used data from AFM images (Figure 4a, b) to examine possible contributions to the greater fluorescence emission intensity from PCD-NH_2/PDMS in comparison with TCD-NH_2/PDMS. Polymer lengths were quantified for both TCD-

NH_2/HOPG and PCD-NH_2/HOPG (Figure 4c,d). Polymer lengths are typically most clearly resolved at early timepoints; thus, we used AFM images acquired prior to $t_{1/2}$ to compare polymer lengths and number densities (see Supporting Information for description of AFM image analysis).

Histograms of the number average degree of polymerization (Figure 4c) are plotted based on measurements of >650 polymers of each type; since the alkyl chain spacing along the polymer is ~0.45 nm/chain, a polymer 45 nm in length corresponds to a degree of polymeriztion (DP) of 100. Weight-average degree of polymerization (DP_w) is plotted using the total number of polymerized monomers that appear in a polymer of that DP (values on the y-axis are divided by 1000). See the Supporting Information for more discussion of calculations. Average PCD-NH_2 polymer lengths are greater than those for TCD-NH_2. (DP_w(PCD-NH_2) = 271, DP_w(TCD-NH_2) = 174). Polymer lengths for the 25- and 23-carbon amine sPDAs reverse the trend observed for carboxylic acids, in which the *shorter* terminal chain segment result in *longer* average polymer lengths (DP_w(PCD-COOH) = 118, and DP_w(TCD-COOH) = 248) at low conversion.[16]

Calculations of probability of sPDA transfer to PDMS based on PDA length. Both classes of monolayers ultimately appear to reach full conversion to polymer, based on AFM imaging (see Supporting Information). However, the fluorescence emission for TCD-NH_2/PDMS remains lower than that for PCD-NH_2/PDMS at the endpoint (I(TCD-NH_2) ≈ 0.6 * I(PCD-NH_2)). Thus, we considered the possibility that shorter polymer lengths (lower DP) for TCD-NH_2 may decrease the probability of PDA transfer.

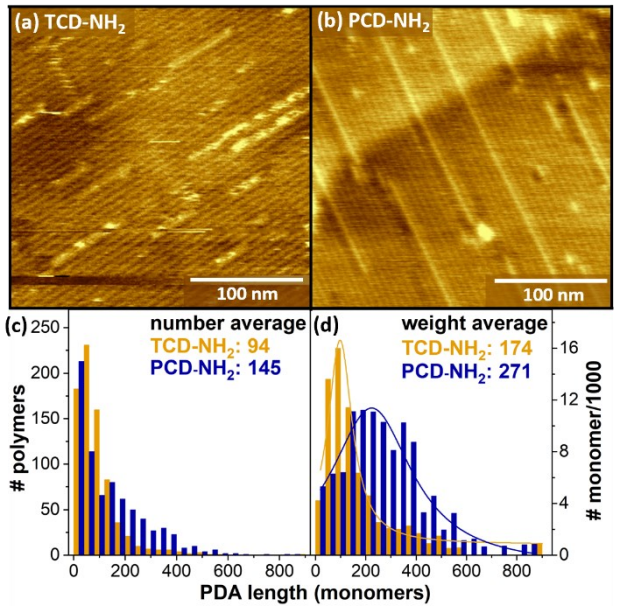

Figure 4. (a, b) AFM images of polymerized (a) TCD-NH_2 and (b) PCD-NH_2 at low conversion timpoints; (c, d) Distribution of polymer lengths of PCD-NH_2 and TCD-NH_2.

In Figure 5, we used the polymer lengths measured for histograms in Figure 4 to predict fractional transfer ($P_{transfer}$) of TCD-NH_2 and PCD-NH_2. Our calculations were based on a range of possible assumptions regarding the probability of PDMS crosslinking to each PDA unit (p_{rxn}) and the number of PDMS–PDA crosslinks required for exfoliation of the sPDA (n = 1 (blue trace), 2 (gold), 3 (red), 4 (green)); see Supporting Information Figures S11-14 and surrounding discussion. Overall, since the mesh (pore) size of SYLGARD-184 PDMS is ~10 nm (Figure S15), we suggest that the maximum number of crosslinks is likely < 1 per 20 PDA repeat units, since crosslinking must connect the sPDA to the PDMS mesh (Figure 5a). Details of the analysis, including ranges chosen for p_{rxn} and n, are discussed in the Supporting Information.

We then calculated the *ratio* of transfer predicted for TCD-NH_2 *vs.* PCD-NH_2 under each set of values for p_{rxn} and n (Figure 5b, right). For instance, the blue curves in the left panels show that, if only one crosslink is required (n=1), then for p_{rxn} values as low as 0.01, similar amounts of transfer

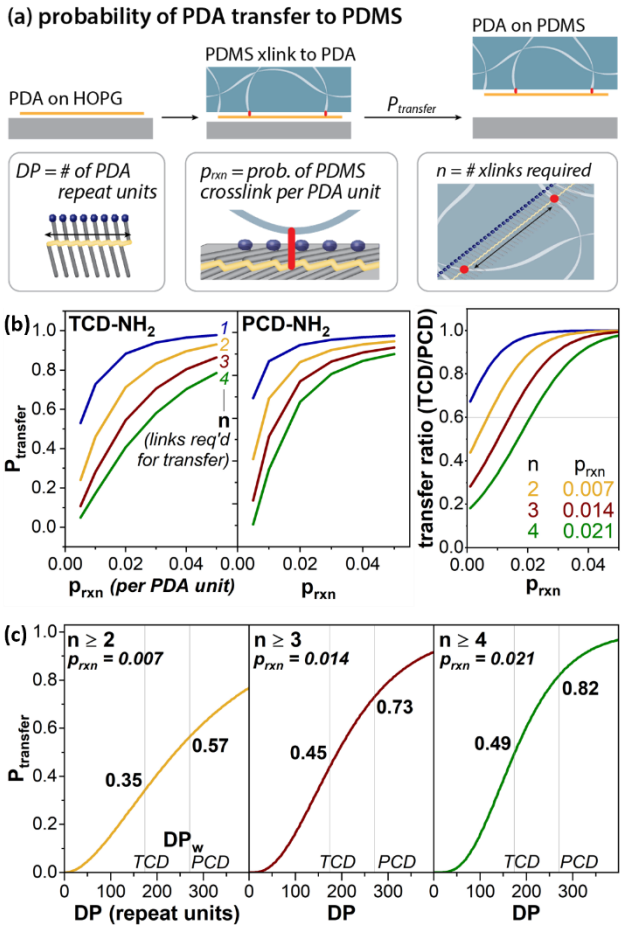

Figure 5. (a) Schematic illustrating structural factors predicted to impact efficiency of sPDA transfer to PDMS. (b) Predicted transfer efficiencies for TCD-NH_2 and PCD-NH_2, within a selected range of per-subunit reaction probabilities (p_{rxn}) and number of crosslinks required for transfer (n). (b, right) Predicted ratio of TCD-NH_2 to PCD-NH_2 transfer. (c) Predicted fractional transfer *vs.* number of sPDA repeat units, if at least 2 crosslinks are required for transfer (left,gold), or if at least 3 (center, red) or 4 (right, green) crosslinks are required.

should be observed for the two molecules (transfer ratio ~1). However, experimentally, lower levels of TCD-NH_2 are observed in comparision with PCD-NH_2. The horizontal grey line in the third graph represents the experimentally observed transfer ratio (~0.6). These calculations suggest that more than 1 crosslink total is required for sPDA exfoliation, since the single-crosslink criterion (n = 1, blue trace) leads to higher

TCD/PCD ratios than those observed experimentally, due to relatively high transfer efficiencies for both molecules. Assuming only 2 crosslinks are required per sPDA transfer, the observed transfer ratio should be achieved for p_{rxn} = 0.007, while for $n \geq 3$ or $n \geq 4$, p_{rxn} would be somewhat higher (0.014 or 0.021, respectively) to achieve the observed transfer ratio.

Figure 5c relates these values to $P_{transfer}$ for average-length polymers of TCD-NH_2 and PCD-NH_2. If a minimum of 2 crosslinks are required for sPDA exfoliation ($n \geq 2$, p_{rxn} = 0.007), the model predicts 35% transfer of average-length TCD-NH_2 polymers, and 57% transfer of average-length PCD-NH_2 polymers. If at least 3 crosslinks are required ($n \geq 3$, p_{rxn} = 0.014), the predicted transfer increases to 45% (TCD-NH_2) and 73% (PCD-NH_2). Finally, if 4 or more crosslinks are required ($n \geq 4$, p_{rxn} = 0.021), the model predicts 49% (TCD-NH_2) and 82% (PCD-NH_2) transfer. Overall, we favor the hypothesis that our typical observations represent the $n \geq 2$ case (Figure 5c, left). Together, these experiments point to the potentially substantially role of large ordered molecular domains in transfer efficiency, allowing for greater average polymer lengths.

Applications of -NH_2 functional arrays on PDMS surfaces. One advantage to maximizing surface functionalization with amine sPDAs is that primary amines are good nucleophiles, and can serve either as handles for covalent postfunctionalization of the interface, or in other applications including mediating assembly of inorganic nanocrystals.

PCD-NH2 striped phase monolayers maximize covalent transfer to PDMS in comparison with TCD-NH_2. Here, we examine the use of PCD-NH_2 surfaces to control adsorption of CdSe nanocrystals (Figure 6a). Nanocrystals are synthesized using previously reported procedures (see Experimental Methods) that produce crystals 2.6 ± 0.7 nm in diameter (Figure 6a, inset) with an octylamine ligand shell. Square patterns of striped phases of PCD-NH_2 on PDMS (Figure 6a) were prepared by microcontact printing (μCP) striped phase PCD-NH_2 on HOPG, then transferring to PDMS (see Experimental Methods in the Supporting Information for more detailed descriptions of each step, including nanocrystal emission spectra in solution, Figure S16).

Prior to nanocrystal exposure, square patterns are visible in AFM phase images (Figure 6b) and in fluorescence emission with excitation in the blue range (440–460 nm) (Figure 6d, top). No emission is visible with excitation in the UV range (330–350 nm) (Figure 6d, bottom). Following exposure to solutions of CdSe NC in cyclohexane, increased phase contrast is visible in AFM images (Figure 6c); modest changes in surface topography are also observed (Figure 6c, inset), though these are irregular as the nanocrystals are not large relative to PDMS pore sizes. Stronger fluorescence emission is visible under both blue and UV excitation (Figure 6e top and bottom, respectively). Spectral imaging (Figure 6f,g) illustrates an ~10x increase in integrated emission intensity with both 488-nm and 405-nm excitation (green and blue traces, respectively). Alkyl carboxylic acids can also act as ligands for CdSe nanocrystals, and COOH striped phases also pattern nanocrystal adsorption (Figure S17); nanocrystals do not adsorb to bare PDMS (Figure S18).

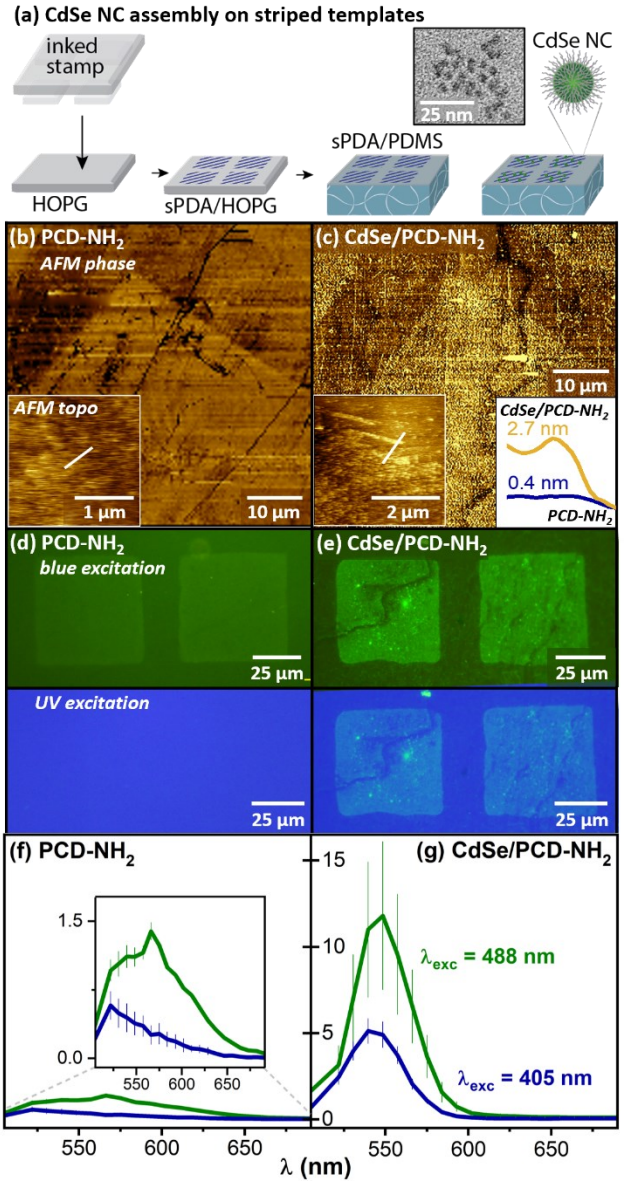

Figure 6. (a) Schematic of nanocrystal binding to PCD-NH_2/PDMS. (a,inset) TEM image of CdSe nanocrystals used in adsorption experiment. (b,c) AFM phase images of (b) PCD-NH_2/PDMS and (c) CdSe/PCD-NH_2/PDMS. Inset in (c) shows line scans acquired in highlighted areas of topography images shown in (b) and (c). (d,e) Fluorescence images of (d) PCD-NH_2/PDMS and (e) CdSe/PCD-NH_2/PDMS under blue excitation (top) and UV excitation (bottom). (f,g) Fluorescence emission spectra of functionalized areas of (f) PCD-NH_2/PDMS and (g) CdSe/PCD-NH_2/PDMS with 488-nm excitation (green traces) and 405-nm excitation (blue traces).

Spectral emission intensities of μCP-patterned PCD-NH_2 (Figure 6f, ~2 a.u. above baseline at full conversion) are noticeably lower than those from PCD-NH_2 sPDAs prepared by LS transfer (Figure 3c, bottom, ~10 a.u. above baseline at

full conversion), which is reasonable, given the smaller domain structures typically observed in microcontact printing. If transfer is consistent with the model developed in Figure 5, this

would correspond to ~12% transfer of the μCP-sPDA layer, and a DP ~100 (*vs.* ~60% transfer and DP 271 for the LS-sPDA layers analyzed in Figure 5). Ongoing work examines strategies for increasing transfer for shorter sPDAs by increasing p_{rxn}.

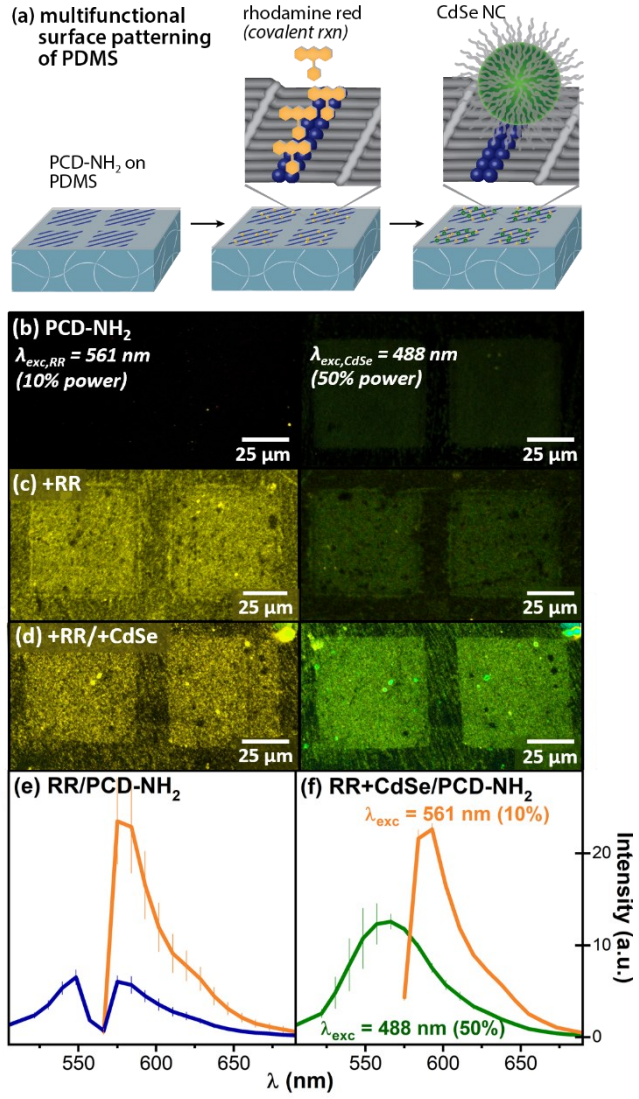

Figure 7. (a) Schematic of sequential functionaliztion of striped PCD-NH_2/PDMS. (b) PCD-NH_2/PDMS (c) PCD-NH_2 + RR/PDMS, and (d) PCD-NH_2 + RR + CdSe/PDMS, imaged with λ_{exc} = 561 nm, 10 % laser power (left images), and with λ_{exc} = 488 nm, 50% laser power (right images) (e) Fluorescence spectra of RR/PCD-NH_2/PDMS and (f) RR + CdSe/PCD-NH_2/PDMS with λ_{exc} = 561 nm (orange traces) and 488 nm (green traces).

Experimental Methods in Supporting Information). Fluorescence images of bare PCD-NH_2 (Figure 7b), PCD-NH_2+RR (Figure 7c), and PCD-NH_2+RR+CdSe (Figure 7d) were acquired at a wavelength chosen to excite RR (λ_{exc} = 561 nm, 10% laser power, left images) and at a wavelength chosen to excite the CdSe nanocrystals (λ_{exc} = 488 nm, 50% laser power, right images). In images of bare PCD-NH_2, square patterns are not visible at the RR excitation conditions, even with contrast enhancement. Squares of PCD-NH_2 are weakly visible under CdSe excitation conditions, which use the same excitation wavelength as that for sPDA imaging (488 nm), although at lower power (50% vs 100%).

Following reaction with RR, square patterns are visible under 561-nm excitation (Figure 7c, left), while contrast is only modestly increased at 488 nm (Figure 7c, right). Significant background fluorescence is observed at 561 nm, even after vigorous washing, consistent with some diffusion of RR into PDMS pores. After further exposure to CdSe, similar contrast is observed at 561 nm (potentially with decreased background fluorescence), while emission at 488 nm increases. The diameter of CdSe NCs with their alkyl ligand shells is similar to PDMS pore diameters (~10 nm), consistent with the lower levels of background fluorescence observed at 488 nm following CdSe exposure, in comparison with background at 561 nm following RR functionalization.

CONCLUSION

Here, we have examined the polymerization and transfer of nm-resolution patterns of alkylamines on HOPG to the surface of PDMS. Using a combination of single-polymer and microscopic measurements, we quantify relationships betweens PDA length and transfer to PDMS, establishing approximate bounds on reaction efficiency and the number of PDMS–sPDA linkages required for transfer. This refines the understanding provided by our previous work, which illustrated that the amount of PDA transfer from HOPG to PDMS increases with the extent of polymerization on HOPG. Following transfer, we illustrate that such patterns can be used to promote both covalent functionalization with fluorescent dyes and adsorption of CdSe nanocrystals with alkyl ligand shells. Overall, our findings here establish criteria for polymer lengths that lead to effective nm-scale patterning of PDMS, and suggest that both alkyl chains and polar headgroups can play important roles in controling adsorption to the PDMS surface.

EXPERIMENTAL METHODS

Materials. 10,12-pentacosadiynoic acid (⩾ 98 %), 10,12-tricosadiynoic acid (⩾98 %), Jones reagent (2M in aq. H_2SO_4), iodine (99.8 %), oxalyl chloride (⩾ 99 % purity), lithium aluminum hydride ($LiAlH_4$, 95 % purity), anhydrous dichloromethane (DCM, ⩾ 99.8 % purity), N-bromosuccinimide (⩾ 99 %), tetrahydrofuran (⩾ 99.9 %), copper chloride (99.5 %), copper(I) iodide (98 %), silver nitrate (⩾ 99.0 %), morpholine (99 %), hydroxylamine hydrochloride (98 % and 99.999 %), ethylamine solution (66.0 – 72.0 % in H_2O), sulfuric acid (95.0–98.0 %), sodium thiosulfate, sodium bicarbonate, and anhydrous sodium sulfate (⩾99.0 % purity), cadmium oxide (CdO, 99.99 % trace metals basis), selenium (100 mesh, ⩾ 99.5% trace metals basis), trioctylphosphine oxide (TOPO, 99 %), trioctylphosphine (TOP) (technical grade, 90 %), were all purchased from MilliporeSigma (St. Louis, MO) and used as received. n-Octadecylphosphonic acid (ODPA, 97 %) was purchased from Alfa Aesar (Ward Hill, MA). Rhodamine Red-X succinimidyl ester and solvents, including N,N-dimethylformamide (⩾99.8 %), acetone (>99.5 %), methanol (>99.5 %), ethyl acetate (>99.5 %), diethyl ether (anhydrous), hexanes and toluene were purchased from Fisher Scientific (Hampton, NH) and used as received. Potassium hydroxide, sodium hydroxide (97% purity) and heptane (99.0 %) were purchased from Fisher

Scientific (Hampton, NH). aq. ammonium hydroxide (28-30% w/w) was purchased from LabChem Inc (Zelienople, PA). AFM probes, Bruker RFESP-75 (0.01–0.025 Ω·cm Antimony (n)-doped Si, nominal force constant 3 N/m and radius of curvature <12 nm) were purchased from Bruker AFM Probes (Camarillo, CA). Highly oriented pyrolytic graphite (HOPG) substrates, grade ZYB, were purchased from SPI Supplies (West Chester, PA). 25-mm PTFE syringe filters were acquired from VWR (Radnor, PA). Buffers with pH 2 (sodium chloride, citric acid and hydrochloride acid) and pH 11 (sodium borate and potassium chloride) were purchased from Honeywell Fluka (Charlotte, NC). Milli-Q water (⩾18.2 MΩ · cm resistivity) was used in all experiments where water was required.

General procedure for the synthesis of 10,12-diynamine from 10,12-diynoic acids. 10,12-pentacosaalkyldiynamine (PCD-NH_2) and 10,12-tricosaalkyldiynamine (TCD-NH_2) were prepared from 10,12-diynoic acids (*i.e.,* 10,12-pentacosadiynoic acid (PCDA) and 10,12-tricosadiynoic acid (TCDA), respectively) using a modification of previously reported literature procedures,[37-39] described briefly here. First, the 10,12-diynoic acid (1 eq) was dissolved in anhydrous DCM under N_2 atmosphere. Oxalyl chloride (1.3 eq) and N,N-dimethylformamide (DMF) (2 drops) were added to the solution. The reaction mixture was stirred at room temperature overnight and concentrated under reduced pressure to obtain the 10,12-diynoyl chloride as a yellow oil; the product was used for the next step without further purification. Next, in a round-bottom flask, 28–30% aqueous ammonium hydroxide (1.3 eq) was added. 10,12-Diynoyl chloride (1 eq) was dissolved in THF and the resulting solution was added to the ammonium hydroxide solution at 0 °C. The reaction mixture was stirred at room temperature for 6 h. The product was extracted with DCM (3 × 50 ml) and the combined organic extract was dried over anhydrous Na_2SO_4. The DCM was evaporated under reduced pressure to yield 10,12-diynoyl amide as white solid. 10,12-Diynoyl amide (1 eq) was placed in a round-bottom flask. Anhydrous diethyl ether was added to the flask under N_2 atmosphere, yielding a white suspension. Subsequently, $LiAlH_4$ (10 eq) was added to the suspension at 0 °C and the reaction mixture was stirred at room temperature for 20 h. After the reaction was complete, the mixture was cooled to 0 °C and treated with sequential dropwise addition of water, aqueous NaOH (15% w/w) and water. The mixture was filtered to remove inorganic impurities. Finally, the filtrate was dried over anhydrous Na_2SO_4 to yield the 10,12-alkyldiynamine as a white solid.

Covalent transfer of striped phase polydiacetylene layers from HOPG to PDMS. Transfer of alkyldiynamine monolayers from HOPG to PDMS was performed using minor modifications of a protocol we developed previously for low-temperature transfer of COOH sPDAs.[14,16] SYLGARD 184 silicone base and crosslinker (curing agent) were mixed in a 10:1 (w/w) ratio. The mixture was stirred for 10 min to maximize homogeneity in distribution of the components, before pouring the PDMS mixture over HOPG substrates functionalized with alkyldiynamine monolayers. The PDMS-coated substrates were placed in a vacuum chamber for 30 min to remove bubbles. Subsequently, PDMS-coated substrates were cured in an oven at 38 °C for 39 h; the relatively long curing schedule at low temperature was chosen to avoid thermal polymerization of alkyldiynamines. Exfoliation of the cured PDMS from the HOPG substrates yielded PDMS surfaces functionalized with amine sPDAs; these were stored in closed sample holders under ambient conditions prior to fluorescence characterization.

Atomic force microscopy (AFM) imaging. A Veeco Multi-Mode with a Nanoscope V controller, or Veeco Dimension (Bruker Instruments, Billerica, MA) was used to acquire AFM images in tapping mode, using Bruker RFESP-75 tips (nominal force constant 3 N/m and radius of curvature <12 nm) in an ambient environment.

Confocal fluorescence microscopy and spectral imaging. Fluorescence images and emission spectra were acquired using a Zeiss LSM 880 Axio Examiner upright confocal microscope, under the excitation of a 488-nm Ar laser at 100% power, focused through a 20x objective (plan-apochromatic, dry, NA = 0.80) with a 0.17-mm glass cover slip placed on the sample. Emitted light was detected by a 32-channel GaAsP spectral photomultiplier detector with a pinhole size set to 1 Airy unit. Fluorescence images were collected at a resolution of 2856 × 718 pixels with 8-bit depth. Scans were acquired unidirectionally and averaged 16 times per line, with a dwell time of 11.75 μs/pixel. Emission spectral data were collected from 495–691 nm (bin centered values) with 8.9-nm resolution.

ASSOCIATED CONTENT

Supporting Information

This material is available free of charge via the Internet at http://pubs.acs.org. Detailed materials and experimental methods, large AFM and SEM images of PCD-NH_2 and TCD-NH_2, AFM images of PCD-NH_2 and TCD-NH_2 at polymerization timepoints, large fluorescence images of PCD-NH_2 and TCD-NH_2 at polymerization timepoints, data analysis of fluorescence images, calculation of PDMS transfer probabilities of polymers, AFM images of PDMS pore structure, spectra and fluorescence images related to CdSe NP adsorption on functionalized PDMS

AUTHOR INFORMATION

Corresponding Author

*Address correspondence to: claridge@purdue.edu

Author Contributions

Notes

The authors declare no competing financial interests.

ACKNOWLEDGMENT

SAC acknowledges support through an NSF grant, NSF-CHE-MSN 2108966. Instrumentation in the Purdue Imaging Facility was utilized for optical microscopy experiments.

REFERENCES

1. Buluta, I.; Ashhab, S.; Nori, F. Natural and Artificial Atoms for Quantum Computation. *Rep. Prog. Phys.* **2011,** *74*, 104401.

2. Barredo, D.; Lienhard, V.; de Leseleuc, S.; Lahaye, T.; Browaeys, A. Synthetic Three-Dimensional Atomic Structures Assembled Atom by Atom. *Nature* **2018,** *561*, 79-82.

3. Hubbell, J. A.; Lutolf, M. P. Synthetic Biomaterials as Instructive Extracellular Microenvironments for Morphogenesis in Tissue Engineering. *Nat. Biotechnol.* **2005,** *23*, 47-55.
4. Rabe, J. P.; Buchholz, S. Commensurability and Mobility in 2-Dimensional Molecular Patterns on Graphite. *Science* **1991,** *253*, 424-427.
5. Cyr, D. M.; Venkataraman, B.; Flynn, G. W. Stm Investigations of Organic Molecules Physisorbed at the Liquid-Solid Interface. *Chem. Mater.* **1996,** *8*, 1600-1615.
6. Groszek, A. J. Preferential Adsorption of Long-Chain Normal Paraffins on Mos_2, Ws_2 and Graphite from N-Heptane. *Nature* **1964,** *204*, 680.
7. de la Rosa, C. J. L.; Phillipson, R.; Teyssandier, J.; Adisoejoso, J.; Balaji, Y.; Huyghebaert, C.; Radu, I.; Heyns, M.; De Feyter, S.; De Gendt, S. Molecular Doping of Mos_2 Transistors by Self-Assembled Oleylamine Networks. *Appl. Phys. Lett.* **2016,** *109*, 253112.
8. Davis, T. C.; Russell, S. R.; Claridge, S. A. Edge-on Adsorption of Multi-Chain Functional Alkanes Stabilizes Noncovalent Monolayers on Mos_2. *Chem. Commun.* **2018,** *54*, 11709-11712.
9. Whitesides, G. M. Soft Robotics. *Angew. Chem., Int. Ed.* **2018,** *57*, 4258-4273.
10. Heikenfeld, J.; Jajack, A.; Rogers, J. A.; Gutruf, P.; Tian, L.; Pan, T.; Li, R.; Khine, M.; Kim, J.; Wang, J.; Kim, J. Wearable Sensors: Modalities, Challenges, and Prospects. *Lab Chip* **2018,** *18*, 217-248.
11. Kyburz, K. A.; Anseth, K. S. Synthetic Mimics of the Extracellular Matrix: How Simple Is Complex Enough? *Ann. Biomed. Eng.* **2015,** *43*, 489-500.
12. Bang, J. J.; Rupp, K. K.; Russell, S. R.; Choong, S. W.; Claridge, S. A. Sitting Phases of Polymerizable Amphiphiles for Controlled Functionalization of Layered Materials. *J. Am. Chem. Soc* **2016,** *138*, 4448-4457.
13. Davis, T. C.; Bechtold, J. O.; Hayes, T. R.; Villarreal, T. A.; Claridge, S. A. Hierarchically Patterned Striped Phases of Phospholipids: Toward Controlled Presentation of Carbohydrates. *Faraday Discuss.* **2019,** *219*, 229-243.
14. Davis, T. C.; Bechtold, J. O.; Shi, A.; Lang, E. N.; Singh, A.; Claridge, S. A. One Nanometer Wide Functional Patterns with a Sub-10 Nanometer Pitch Transferred to an Amorphous Elastomeric Material. *ACS Nano* **2021,** *15*, 1426-1435.
15. Bechtold, J. O.; Arango, J. C.; Shi, A.; Singh, A.; Claridge, S. A. Striped Poly(Diacetylene) Monolayers Control Adsorption of Polyelectrolytes and Proteins on 2D Materials and Elastomers. *ACS Appl. Nano Mater.* **2021,** *4*, 7037-7046.
16. Shi, A.; Villarreal, T. A.; Singh, A.; Hayes, T. R.; Davis, T. C.; Brooks, J. T.; Claridge, S. A. Plenty of Room at the Top: A Multi-Scale Understanding of Nm-Resolution Polymer Patterning on 2D Materials. *Angew. Chem., Int. Ed.* **2021,** *60*, 25436-25444.
17. Giridharagopal, R.; Kelly, K. F. Stm-Induced Desorption of Polydiacetylene Nanowires and Reordering Via Molecular Cascades. *J. Phys. Chem. C* **2007,** *111*, 6161-6166.
18. Grim, P. C. M.; De Feyter, S.; Gesquiere, A.; Vanoppen, P.; Rucker, M.; Valiyaveettil, S.; Moessner, G.; Mullen, K.; De Schryver, F. C. Submolecularly Resolved Polymerization of Diacetylene Molecules on the Graphite Surface Observed with Scanning Tunneling Microscopy. *Angew. Chem., Int. Ed.* **1997,** *36*, 2601-2603.
19. Okawa, Y.; Aono, M. Materials Science - Nanoscale Control of Chain Polymerization. *Nature* **2001,** *409*, 683-684.
20. Endo, O.; Ootsubo, H.; Toda, N.; Suhara, M.; Ozaki, H.; Mazaki, Y. Phase Transition of a Single Sheet of Sashlike Polydiacetylene Atomic Sash on a Solid Surface. *J. Am. Chem. Soc.* **2004,** *126*, 9894-9895.
21. Okawa, Y.; Akai-Kasaya, M.; Kuwahara, Y.; Mandal, S. K.; Aono, M. Controlled Chain Polymerisation and Chemical Soldering for Single-Molecule Electronics. *Nanoscale* **2012,** *4*, 3013-3028.
22. Verveniotis, E.; Okawa, Y.; Watanabe, K.; Taniguchi, T.; Taniguchi, T.; Osada, M.; Joachim, C.; Aono, M. Self-Sensitization and Photo-Polymerization of Diacetylene Molecules Self-Assembled on a Hexagonal-Boron Nitride Nanosheet. *Polymers* **2018,** *10*, 206.
23. Wegner, G. Topochemical Polymerization of Monomers with Conjugated Triple Bonds. *Makromol. Chem.* **1972,** *154*, 35-48.
24. Tieke, B.; Graf, H. J.; Wegner, G.; Naegele, B.; Ringsdorf, H.; Banerjie, A.; Day, D.; Lando, J. B. Polymerization of Monolayer and Multilayer Forming Diacetylenes. *Colloid Polym. Sci.* **1977,** *255*, 521-531.
25. Rawiso, M.; Aime, J. P.; Fave, J. L.; Schott, M.; Muller, M. A.; Schmidt, M.; Baumgartl, H.; Wegner, G. Solutions of Polydiacetylenes in Good and Poor Solvents: A Light and Neutron Scattering Study. *J. Phys.* **1988,** *49*, 861-880.
26. Bassler, H., *Photopolymerization of Diacetylenes*. Springer: Heidelberg, 1984; Vol. 63.
27. Galanina, O. E. Glycochip: Multiarray for the Study of Carbohydrate-Binding Proteins. *Lab Chip* **2003,** *3*, 260.
28. Maier, G. P.; Rapp, M. V.; Waite, J. H.; Israelachvili, J. N.; Butler, A. Adaptive Synergy between Catechol and Lysine Promotes Wet Adhesion by Surface Salt Displacement. *Science* **2015,** *349*, 628-632.
29. Noel, S.; Liberelle, B.; Robitaille, L.; De Crescenzo, G. Quantification of Primary Amine Groups Available for Subsequent Biofunctionalization of Polymer Surfaces. *Bioconj. Chem.* **2011,** *22*, 1690-1699.
30. Cen, L.; Neoh, K. G.; Kang, E. T. Surface Functionalization of Electrically Conductive Polypyrrole Film with Hyaluronic Acid. *Langmuir* **2002,** *18*, 8633-8640.
31. Davis, T. C.; Bang, J. J.; Brooks, J. T.; McMillan, D. G.; Claridge, S. A. Hierarchical Noncovalent Functionalization of 2D Materials by Controlled Langmuir-Schaefer Conversion. *Langmuir* **2018,** *34*, 1353-1362.
32. Bang, J. J.; Porter, A. G.; Davis, T. C.; Hayes, T. R.; Claridge, S. A. Spatially Controlled Noncovalent Functionalization of 2D Materials Based on Molecular Architecture *Langmuir* **2018,** *34*, 5454-5463.
33. Okawa, Y.; Aono, M. Linear Chain Polymerization Initiated by a Scanning Tunneling Microscope Tip at Designated Positions. *J. Chem. Phys.* **2001,** *115*, 2317-2322.
34. Chance, R. R.; Patel, G. N. Solid-State Polymerization of a Diacetylene Crystal: Thermal, Ultraviolet, and Γ-Ray Polymerization of 2,4-Hexadiyne-1,6-Diol Bis-(P-Toluene Sulfonate). *J. Polym. Sci., Polym. Phys. Ed.* **1978,** *16*, 859-881.
35. Yin, S.; Wang, C.; Qiu, X.; Xu, B.; Bai, C. Theoretical Study of the Effects of Intermolecular Interactions in Self-Assembled Long-Chain Alkanes Adsorbed on Graphite Surface. *Surf. Interf. Anal.* **2001,** *32*, 248-252.
36. Patel, G. N.; Chance, R. R.; Turi, E. A.; Khanna, Y. P. Energetics and Mechanism of Solid-State Polymerization of Diacetylenes. *J. Am. Chem. Soc.* **1978,** *100*, 6644-6649.
37. Howarth, N. M.; Lindsell, W. E.; Murray, E.; Preston, P. N. Lipophilic Peptide Nucleic Acids Containing a 1,3-Diyne Function: Synthesis, Characterization and Production of Derived Polydiacetylene Liposomes. *Tetrahedron* **2005,** *61*, 8875-8887.
38. Lee, J. P.; Hwang, H.; Chae, S.; Kim, J.-M. A Reversibly Mechanochromic Conjugated Polymer. *Chem. Commun.* **2019,** *55*, 9395-9398.
39. Pumtang, S.; Siripornnoppakhun, W.; Sukwattanasinitt, M.; Ajavakom, A. Solvent Colorimetric Paper-Based Polydiacetylene Sensors from Diacetylene Lipids. *J. Colloid Interface Sci.* **2011,** *364*, 366-372.

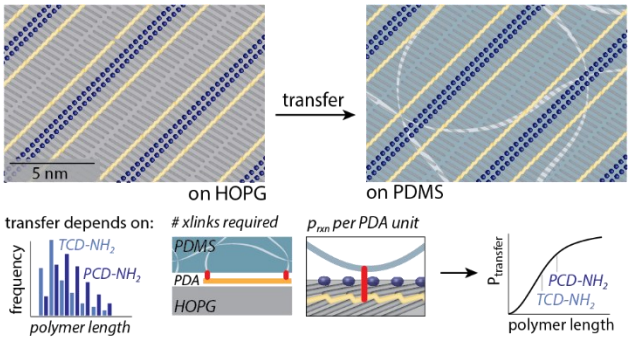
5 nm
transfer
on HOPG
on PDMS
transfer depends on:
xlinks required
p_{rxn} per PDA unit
frequency
TCD-NH2
PCD-NH2
polymer length
PDMS
PDA
HOPG
P transfer
PCD-NH2
TCD-NH2
polymer length